Journal of Alloys and Compounds 1010 (2025) 177570

Contents lists available at ScienceDirect

Journal of Alloys and Compounds

journal homepage: www.elsevier.com/locate/jalcom

Direct and indirect assessment of the elastocaloric properties of cast NiMnTi alloys

Francesca Villa [a,b,*], Elena Villa [b], Nicola Bennato [b], Francesca Passaretti [b], Riccardo Casati [a]

[a] Politecnico di Milano, Mechanical Engineering Department, Milano, Italy
[b] Institute of Condensed Matter Chemistry and Technologies for Energy, National Research Council (CNR ICMATE), Lecco, Italy

ARTICLE INFO

Keywords:
Elastocaloric effect
NiMnTi
Adiabatic ΔT
Isothermal entropy change
Stress-induced martensitic transformation
Coefficient of performance

ABSTRACT

The study of the elastocaloric effect of NiMnTi alloys is a key topic for developing materials for sustainable and efficient solid-state cooling and heating applications. In the current work, the mechanical behavior of two arc melted and heat treated NiMnTi alloys with 15 and 18 at% of Ti has been investigated. The effects of heat treatments and operating conditions on the mechanical and caloric properties of the alloys have been assessed through calorimetric analysis, isothermal stress-strain compressive measurements, and adiabatic tests. To evaluate the caloric performance of the NiMnTi alloys, both experimental and theoretical adiabatic temperature changes have been identified, and the isothermal entropy change involved in the stress-induced martensitic transformation has been computed from the discrete integration of the stress-strain curves. The NiMnTi alloys treated at 900 °C exhibited better caloric performance than those treated at 1000°C. Specifically, the sample that achieved the highest experimental positive and negative ΔT values (10.2 °C and −12.6 °C, respectively) was the NiMnTi alloy with 15 at% of Ti and heat treated at 900 °C. This study provides a detailed analysis of the physical properties, functionality, and caloric properties of polycrystalline NiMnTi fabricated through a melting process, considering its potential use in solid-state cooling and heat pumping technologies.

1. Introduction

The elastocaloric cooling is one of the most promising and effective solid-state alternatives to traditional vapor compression methods [1–3]. The main advantages of elastocaloric technologies include compactness and simplicity of operation [4], high efficiency [5], and low environmental impact [6–8], as they do not involve harmful fluids, such as hydrofluorocarbons. Shape memory alloys (SMAs) are suitable materials for the development of elastocaloric systems [9–11], since they are characterized by a first-order reversible solid-state transformation known as thermoelastic martensitic transformation (TMT), which involves high latent heat [12]. It is possible to induce the martensitic transformation by applying a load to a SMA in the austenitic parent phase under adiabatic conditions, i.e. without heat dissipation towards the environment. By removing the load, the endothermic inverse transformation occurs, and the material cools down [13–18]. The heat generated can be stored and utilized for various applications, potentially involving different thermodynamic cycles [19]. Experimentally, quasi-adiabatic loading conditions are achieved when the material is deformed rapidly, with strain rates higher than 0.05 s^{-1} [14].

The elastocaloric effect of shape memory alloys can be described by several parameters that indicate, either directly or indirectly, the heating and cooling capacity of the material under different loading conditions [9,13,14,16,20]. Based on the calorimetric properties of the material corresponding to the direct austenite-to-martensite transformation, the maximum temperature change (ΔT_{ad}^{th}), that can be achieved at an operating temperature T and related to the direct transition (i.e. during loading) is expressed as follows:

$$\Delta T_{ad}^{th} = \frac{\Delta S_{A-to-M}}{c_p} T = \frac{\Delta H_{A-to-M}}{T_0 \; c_p} T \quad (1)$$

where $\Delta S_{A\text{-}to\text{-}M}$ is the entropy change associated with the martensitic transformation, $\Delta H_{A\text{-}to\text{-}M}$ is the enthalpy involved in the thermally-induced martensitic transformation, c_p is the specific heat, T is the operating temperature for the elastocaloric experiment, and T_0 is defined as $(M_s + A_f)/2$, where Ms is the Martensite Start temperature and Af is the Austenite Finish temperature [12]. This maximum ΔT can be compared with the value experimentally measured on the sample surface by adiabatic measurements, i.e. ΔT_{ad}^{exp}.

* Corresponding author at: Politecnico di Milano, Mechanical Engineering Department, Milano, Italy.
E-mail address: francesca.villa@icmate.cnr.it (F. Villa).

https://doi.org/10.1016/j.jallcom.2024.177570
Received 9 September 2024; Received in revised form 29 October 2024; Accepted 12 November 2024
Available online 13 November 2024

A second parameter commonly used to describe the elastocaloric behavior of the material is the entropy change in isothermal conditions associated with the stress-induced martensitic transformation, which can be derived from the isothermal stress-strain curves in two ways. In the first case, the ΔS is computed from the Clausius-Clapeyron relationship as follows:

$$|\Delta S_{iso}^{CC}| = \frac{1}{\rho} k_{CC} \varepsilon_{tr} \tag{2}$$

where ρ is the density of the alloy, k_{CC} is the Clausius-Clapeyron coefficient determined from the isothermal stress-strain measurements at increasing temperatures and ε_{tr} is the transformation strain [21]. The second approach relies on the discrete integration of the entire stress-strain curves according to the Maxwell equation:

$$|\Delta S_{iso}^{SS}| = \frac{1}{\rho} \int_0^{\varepsilon} \frac{\partial \sigma}{\partial T} \, d\varepsilon \tag{3}$$

Finally, a coefficient of performance of the caloric material (COP_{mat}) can be defined as the ratio between the heat involved in the stress-induced adiabatic transformation and the work input (W), assuming total work recovery upon unloading. This relationship can be expressed as follows:

$$COP_{mat} = \frac{c \ \Delta T_{ad}^{\exp}}{\frac{1}{\rho} \oint \sigma d\varepsilon} \tag{4}$$

In Eq. 4, the work input is assumed to be the hysteresis loop area of the complete stress-strain curve.

One of the emerging shape memory alloys being explored for elastocaloric applications is the Heusler alloy NiMnTi, which consists solely of elements from the *3d* transition metal group [22,23]. Typically, Heusler alloys are characterized by strong covalent bonding between the constitutive elements due to the *p-d* orbital hybridization, leading to intrinsic brittleness of these intermetallics. In contrast, NiMnTi is characterized by *d-d* orbital hybridization, resulting in a uniform distribution of valence electrons [24–28]. This positively affects the mechanical properties of NiMnTi, which exhibits higher ductility compared to more common NiMn-based alloys, such as NiMnGa and NiMnGa-based quaternary alloys [29–31]. Moreover, the significant unit cell volume change involved in the martensitic transformation is among the material properties that can affect in a positive way the elastocaloric behavior [32].

When it comes to arc-melted NiMnTi alloys, there is a limited number of studies that focus on their physical and elastocaloric properties. In the study reported in [33], it was found that cast $Ni_{50}Mn_{32}Ti_{18}$ samples annealed at 900 °C for 144 hours exhibit an irreversible adiabatic temperature change of 10.7 °C with 3.9 % deformation. In another study [34], NiMnTi samples containing 18 at% Ti and annealed at 950°C for 48 hours exhibited an adiabatic ΔT equal to 17 °C at an applied strain of 7 % and a ΔS equal to 52.9 J kg^{-1} °C^{-1}. It was demonstrated that boron acts as an effective grain refiner and has a positive effect on the elastocaloric properties of both NiMnIn-based alloys [35,36], and NiMnTi ones [37–39] leading to experimentally-measured ΔT values up to 31.5 °C [32]. A few studies [24,34,40,41] investigate the NiMnTi produced by directional solidification methods and correlates microstructural texture with enhanced superelastic properties and elastocaloric effect. Indeed, directionally solidified samples exhibit superior transformation strains up to 4 % and superelastic behavior up to deformations equal to 10 % without residual strains [24]. Moreover, adiabatic ΔT up to 37.3 °C and ΔS up to 50 J kg^{-1} °C^{-1} are reported [34].

In this work, the behavior of two polycrystalline NiMnTi alloys produced by arc melting is described through the evaluation of their elastocaloric parameters, namely ΔT, ΔS, and COP_{mat}. The study investigates how heat treatments affect the elastocaloric characteristics of these alloys, aiming to deepen insights into cast NiMnTi polycrystalline materials. This research builds on our previous work [42] to further explore the physical and functional properties, ultimately looking to advance NiMnTi alloys for use in solid-state cooling and heat pumping technologies.

2. Materials and methods

$Ni_{50}Mn_{35}Ti_{15}$ and $Ni_{50}Mn_{32}Ti_{18}$ alloys were produced by arc melting from high purity metallic elements (electrolytic Ni with purity level of 99.97 % and electrolytic Mn with purity level of 99.5 % by Merck, grade 1 Ti wire (ASTM B348) by Titalia) and the ingots were subjected to six remelting steps under Ar atmosphere [42]. The measured chemical composition of the ingots is reported in reference [42].

The as-cast samples were sealed into quartz vials under argon, heat treated at 900 °C and 1000 °C for 48 and 24 hours, respectively, and water quenched. The obtained samples were labeled as follows: "NMT15_TT900", "NMT15_TT1000", "NMT18_TT900", and "NMT18_TT1000". In a previous work [42] it was found that these heat treatments promoted alloy homogenization, resulting in the dissolution of solidification structures and a narrowing of the TMT temperatures measured by calorimetry. In the case of the heat treatment at 900 °C, Ni-Ti based micrometric precipitates, in particular Ni_3Ti, formed at grain boundaries and within the grains. Conversely, after heat treatment at 1000 °C, no precipitates were observed. Density measurements were carried out by Archimede's method with an analytical balance Ghibertini E50S/2. Calorimetric analysis was performed with a differential scanning calorimeter (DSC25 by TA instruments) at a heating and cooling rate of 10 °C/min. The transformation temperatures were determined at the intersection between the tangent lines at the inflection points of the peaks and the baseline. The samples for the compression tests were cut from the arc melted ingots by means of an abrasive blade and then refined using grinding paper to obtain parallel faces. The final samples had square sections measuring between 2×2 mm^2 and 2.5×2.5 mm^2 with heights ranging from 4 mm to 5 mm. The compressive mechanical measurements were performed by means of an Instron E3000 all-electric dynamic mechanical test instrument equipped with a 3 kN load cell, a magnetic actuator and an optical drive calibrated for the actual working conditions to measure the actuator displacement. Each sample was trained before mechanical tests through consecutive compressive loading-unloading cycles at a strain rate of 1 %/min and with a target strain of 4 % during loading and a target stress of 3 MPa during unloading, at the first test temperature. The number of training cycles was equal to the number of cycles required to achieve complete recovery upon unloading without residual strains. The isothermal measurements were carried out at a strain rate of 1 %/min and with a target strain equal to 4 % upon loading and a target stress equal to 3 MPa upon unloading. The adiabatic measurements were performed at Af +15 °C with strain rates of 150, 400, and 800 %/min. The target loading strains were set to 3 and 4 %, while the target unloading stress was maintained at 3 MPa. After rapid loading and unloading phases, the reached strain was held constant for 40 seconds to promote heat release towards the environment. Five loading-unloading cycles were performed for each combination of applied strain and strain rate. The critical stress for the induction of martensite (σ_{cr}) is evaluated by the intersection of the tangent line to the initial elastic part of the isothermal stress-strain curves and the tangent line to the plateau of martensite formation. Three thin T-type thermocouples (bare wire with diameter of 0.127 mm) were fixed with silver paste directly in the middle of three lateral surfaces of the samples and connected to a high-frequency acquisition system (NI 9212) for the evaluation of the adiabatic ΔT as described in references [43,44].

3. Results

The thermal properties of the two NiMnTi alloys were assessed in a previous work [42] and the enthalpies of the austenite-to-martensite

transformation ($\Delta H_{A\text{-}to\text{-}M}$) and the temperature T_0 derived from the DSC analysis are reported in Table 1. From these data, it was possible to determine, according to Eq. 1, the theoretical adiabatic temperature change (ΔT_{ad}^{th}) associated to the thermally induced transformation between austenite and martensite for each sample. This value corresponds to the maximum achievable temperature change assuming perfect adiabatic conditions and absence of energy losses. The specific heat considered for this calculation is the reference value for the $Ni_{50}Mn_{32}Ti_{18}$ alloy with directionally solidified microstructure [24] corresponding to 0.45 J g^{-1} °C^{-1}. Table 1 shows the computed ΔT_{ad}^{th} and it is possible to notice that the alloy with 15 at% of Ti exhibited the highest theoretical temperature changes. Moreover, for both $NiMnTi_{15}$ and $NiMnTi_{18}$ alloys, the highest ΔT_{ad}^{th} were given by the samples treated at 900 °C.

In addition to the purely thermal approach, the mechanical behavior of the NiMnTi alloys was investigated through compressive isothermal stress-strain tests at different temperatures. Fig. 1 shows the stress-strain curves of the four samples at temperatures ranging between $A_f + 5$ °C and $A_f + 35$ °C. The curves obtained for sample NMT18_TT900 do not completely reach the target strain, but martensite induction plateaus are still clearly visible. It is noticeable that, as expected for austenitic SMAs [12], the critical stress for inducing martensite (σ_{cr}) increased with temperature, whereas the hysteresis between loading and unloading plateaus decreased. Furthermore, higher σ_{cr} were achieved by $NiMnTi_{15}$ alloy with respect to $NiMnTi_{18}$, for the same strain at temperatures close to A_f. Finally, considering the effect of the heat treatment, in the samples treated at 900 °C (Figs. 1(a) and 1(c)) martensite started forming at higher stresses and strains in both the alloys with respect to the samples treated at 1000°C, as can be also noticed from Fig. 2. For all the samples it is noticeable a certain residual strain, which is particularly significant in the curve of NMT15_TT1000.

The trend of the critical stresses with increasing test temperature is represented by the Clausius-Clapeyron coefficient (k_{CC}), which corresponds to the slope of the linear fit of the σ_{cr} versus temperature data. Fig. 2 shows the σ_{cr} vs. temperature behavior for all the NiMnTi samples and k_{CC} values up to 8.3 and 6.3 MPa °C^{-1} were computed for $NiMnTi_{15}$ and $NiMnTi_{18}$ alloys, respectively.

According to Eq. 2, the Clausius-Clapeyron dependence can be used for a preliminary estimation of the entropy change ΔS_{iso}^{CC} involved in the isothermal stress-induced martensitic transformation. The ΔS_{iso}^{CC} of the four samples are listed in Table 2 together with the measured densities (ρ), the transformation strain, the computed k_{CC} coefficients, and the ΔT_{ad}^{CC} calculated according to Eq. 1 replacing ΔS_{A-to-M} with ΔS_{iso}^{CC}. The transformation strain was evaluated by the tangent method considering the slope of the plateau and the elastic regions of the curves.

From the energy standpoint, the best performance is attributed to the NMT15_TT900 sample, which exhibited an ΔS_{iso}^{CC} of 20.2 J kg^{-1} °C^{-1}. Similarly, a slightly higher entropy change was obtained by the NiMnTi18_TT900. Finally, the ΔT computed starting from these data reflected the trend of the ΔS_{iso}^{CC} resulting in values that are lower than the ΔT_{ad}^{th} achieved following an entirely thermal approach.

Further investigation of the entropy changes involved in the stress-induced martensitic transformation (ΔS_{iso}^{SS}) was possible through the discrete integration of the mechanical curves at fixed temperatures, according to Eq. 3 (Fig. 3). For most of the temperatures, the highest ΔS_{iso}^{SS} was achieved at the maximum strain, i.e. 4 % and 3.5 % for $NiMnTi_{15}$ and $NiMnTi_{18}$ alloys, respectively, and the maximum peak value of the ΔS_{iso}^{SS}, i.e. 51 J kg^{-1} °C^{-1}, was achieved by sample NMT18_TT900 at 32.5 °C. As for the entropy results, the samples that underwent heat treatment at 900 °C exhibited slightly higher peak values. Moreover, it can be noticed that the entropy change vs. temperature curves do not exhibit extremely pronounced peaks, especially for the NMT15 alloy. For instance, in the NMT15_TT1000 sample (Fig. 3 (b)), the ΔS_{iso}^{SS} decreased by only 10 % between 162.5°C and 172.5°C. In contrast, the NMT18 alloy exhibited a more variable trend, with sharper ΔS_{iso}^{SS} peaks.

The adiabatic ΔT during compressive adiabatic tests (ΔT_{ad}^{exp}) on four samples at different strain rates (150, 400 and 800 %/min) and strains of 3 % and 4 % (Fig. 4) was measured. Fig. 4(c) shows an example of the mechanical curves and the adiabatic temperature change values for NMT18_TT900. As expected, the ΔT_{ad}^{exp} grew with the strain rate and strain [24]. This is due to the increased formation of martensite and the improved achievement of adiabatic conditions. The curves in Figs. 4(a) and 4(b) do not show the expected plateaus because of the high strain rates [14]. The stresses were higher than those of the isothermal tests for the same strains and increased with the strain rate. This also made hysteresis and residual strains larger. All the other samples showed a similar behavior. Fig. 5 compares the different NiMnTi samples at 4 % strain and 800 %/min strain rate, which were the best conditions to maximize the ΔT_{ad}^{exp}. As observed from the representative temperature profiles, slightly higher temperature changes were achieved upon unloading, particularly for $NiMnTi_{15}$ samples. This phenomenon could be ascribed to several factors, including the different effects of microstructural features such as grain boundaries, as well as the influence of defects or impurities on direct and indirect martensitic transformation, i.e. on martensite nucleation and shrinking, respectively. Additionally, the apparatus used for the tests is more precise in the control of the unloading phase and therefore it is possible that more accurate adiabatic conditions are achieved upon unloading. The highest positive and negative ΔT_{ad}^{exp} values, i.e. 10.2 °C and −12.6 °C, were achieved by the NMT15_TT900 sample (Fig. 5(a)). For the NiMnTi alloy with 18 % of Ti, the best sample was the one heat treated at 900 °C. Note that the temperature on NMT18_TT900 sample surface fluctuated about ± 1 °C around the target temperature, i.e. 25 °C, due to the instability of the thermal chamber, which used nitrogen gas to cool down.

The efficiency of the material under adiabatic cycling is represented by a COP_{mat} that can be calculated from the measured ΔT_{ad}^{exp}, reported in Table 3 for loading, using Eq. 4. The reported ΔT_{ad}^{exp} values are the mean values of the temperature changes obtained upon the five loading cycles performed at 800 % min^{-1} and 4 % of applied strain. Table 3 also shows the work input (W), which is the hysteresis loop area of the complete stress-strain curves, during adiabatic cyclic tests for the four samples. It is known that the value of specific heat varies during the transformation [45]. However, for sake of simplicity, the constant cp value reported in literature [24] was used for the COP_{mat} calculation. The elastocaloric performance of the alloys followed the same trend, with the highest COP_{mat} for the samples treated at 900 °C.

Table 1
Summary of the measured enthalpy changes $\Delta H_{A\text{-}to\text{-}M}$, Af, T_0, T and entropy changes ΔS_{tr} and of the calculated ΔT_{ad}^{th} according to Eq. 1. The data indicated with an asterisk (*) were evaluated in a previous study [42].

Sample	$\Delta H_{A\text{-}to\text{-}M}$ (J g^{-1}) *	Af (°C) *	T_0 (°C) *	ΔS_{tr} (J kg^{-1} °C^{-1})	T (°C)	ΔT_{ad}^{th} (°C)
NMT15_TT900	34.7	121.5	114.5	87.0	140	82.1
NMT15_TT1000	31.6	152.7	143.7	74.1	170	74.6
NMT18_TT900	21.4	8.1	0.3	78.2	25	51.8
NMT18_TT1000	18.4	29.9	17.9	63.2	45	44.6

4. Discussion

From the thermal standpoint, the two studied alloys show promising elastocaloric performance, as reported in Table 1, and, in particular, the ΔT_{ad}^{th} values obtained for $NiMnTi_{15}$ alloy are significantly higher with respect to those typical of shape memory alloys [9]. In fact, a maximum $\Delta T = 35$ °C is obtained for NiMnTi alloys with directionally-solidified microstructure from theoretical evaluations [24]. The theoretical

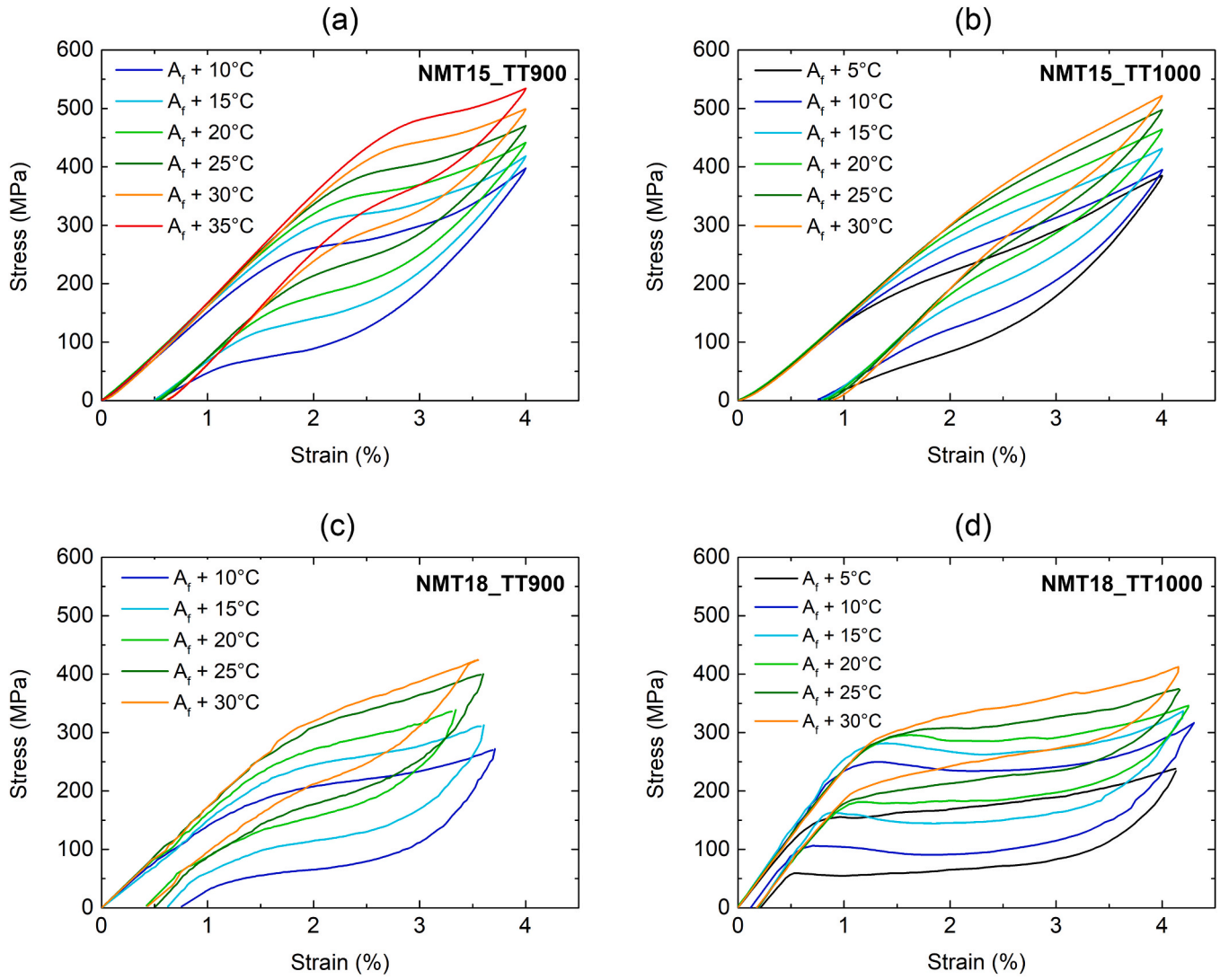

Fig. 1. Compressive isothermal stress-strain curves for samples NMT15_TT900 (a), NMT15_TT1000 (b), NMT18_TT900 (c) and NMT18_TT1000 (d).

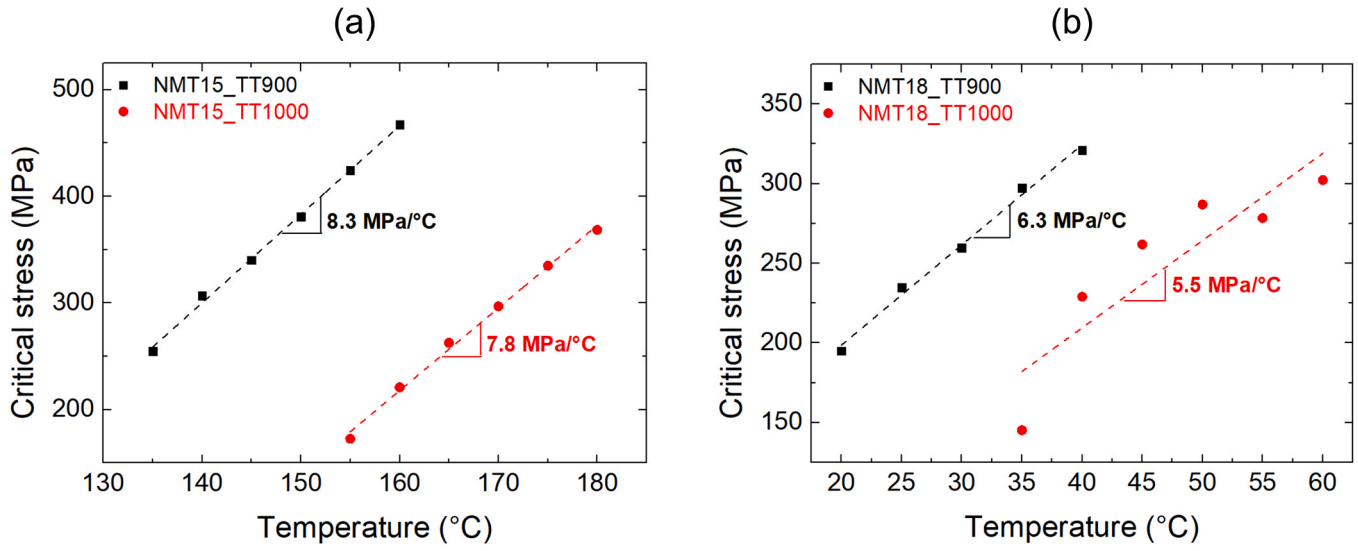

Fig. 2. Critical stresses (σ_{cr}) versus temperature for NMT_{15} (a) and NMT_{18} (b) alloys. The slopes of the linear fitting, i.e. the Clausius-Clapeyron coefficients (k_{CC}), are reported for each sample.

Table 2
Summary of the measured densities ρ, transformation strains ε_{tr} and k_{CC} coefficients, and of the calculated ΔS_{iso}^{CC} and ΔT_{ad}^{CC}.

sample	ρ (g cm^{-3})	k_{CC} (MPa °C^{-1})	ε_{tr}	ΔS_{iso}^{CC} (J kg^{-1} °C^{-1})	ΔT_{ad}^{CC} (°C)
NMT15_TT900	7.1	8.3	0.0173	20.2	18.6
NMT15_TT1000	7.1	7.8	0.017	18.7	18.3
NMT18_TT900	7.2	6.3	0.018	15.7	10.4
NMT18_TT1000	7.2	5.5	0.0195	14.9	10.5

values obtained in the current work (up to 82.1 and 58.1 °C for $NiMnTi_{15}$ and $NiMnTi_{18}$ respectively), especially for the alloy with 15 % of Ti, clearly overestimate ΔT, being much higher than those directly measured on the samples, which correspond to 10.2 and 9.8 °C for $NiMnTi_{15}$ and $NiMnTi_{18}$ respectively. The origin of these discrepancy lies on the evaluation of the enthalpies obtained from the calorimetric data, that result in extremely high enthalpy change values especially for $NiMnTi_{15}$ alloy. However, the ΔT_{ad}^{th} values provide a first indication of the superior heating and cooling capacity of the alloy with 15 % of Ti. Moreover, research has indicated that relying solely on the thermal method leads to an overestimation of the elastocaloric potential in alloys, whereas parameters obtained from mechanical test analysis are more reliable [11,30]. Indeed, for the elastocaloric applications, it is essential to take into account the interplay between the thermal properties of the alloy and the mechanism of the martensitic transformation induced by mechanical stress. Therefore, the ΔT values were further estimated from the mechanical data and then experimentally measured on the samples in adiabatic loading conditions. An overall comparison of the ΔT obtained by these direct and indirect approaches is presented in Fig. 6.

The ΔT_{ad}^{CC} were lower than ΔT_{ad}^{th} values, due to the fact that in one case the martensitic transformation is stress induced, in the other case it is thermally induced. Indeed, it is possible that during the formation of the single variant stress induced martensite with the application of a stress field, additional dissipative effects could arise [11] and this can result in a lower evaluation of the caloric effect. Moreover, the relatively limited transformation strains observed in the samples compared to those with the same composition but more favorable microstructures, such as directionally solidified alloys with preferential grain orientation, could hinder the full expression of the elastocaloric capability of the material under investigation in this study. This limitation may contribute to the discrepancy between the elastocaloric performance evaluated through calorimetry and mechanical tests. In the $NiMnTi_{18}$ alloy, the ΔT_{ad}^{CC} values better approach the experimental ones compared to the $NiMnTi_{15}$ alloy. The experimental measurements of ΔT_{ad}^{exp} evidenced the effect of the combination of the actual thermal properties (e.g. specific heat and thermal conductivity) and mechanical properties of the samples together with the experimental conditions such as applied strain rates and sample geometry. In fact, the measured ΔT_{ad}^{exp} (Fig. 5) are lower than the theoretical ΔT because of several factors. One reason is that the loading conditions are not completely adiabatic, because the high deformation rate only approximates the adiabatic condition, so some heat transfer to the environment might occur [14]. Moreover, the experimental setup is composed of metallic fixtures that further promote

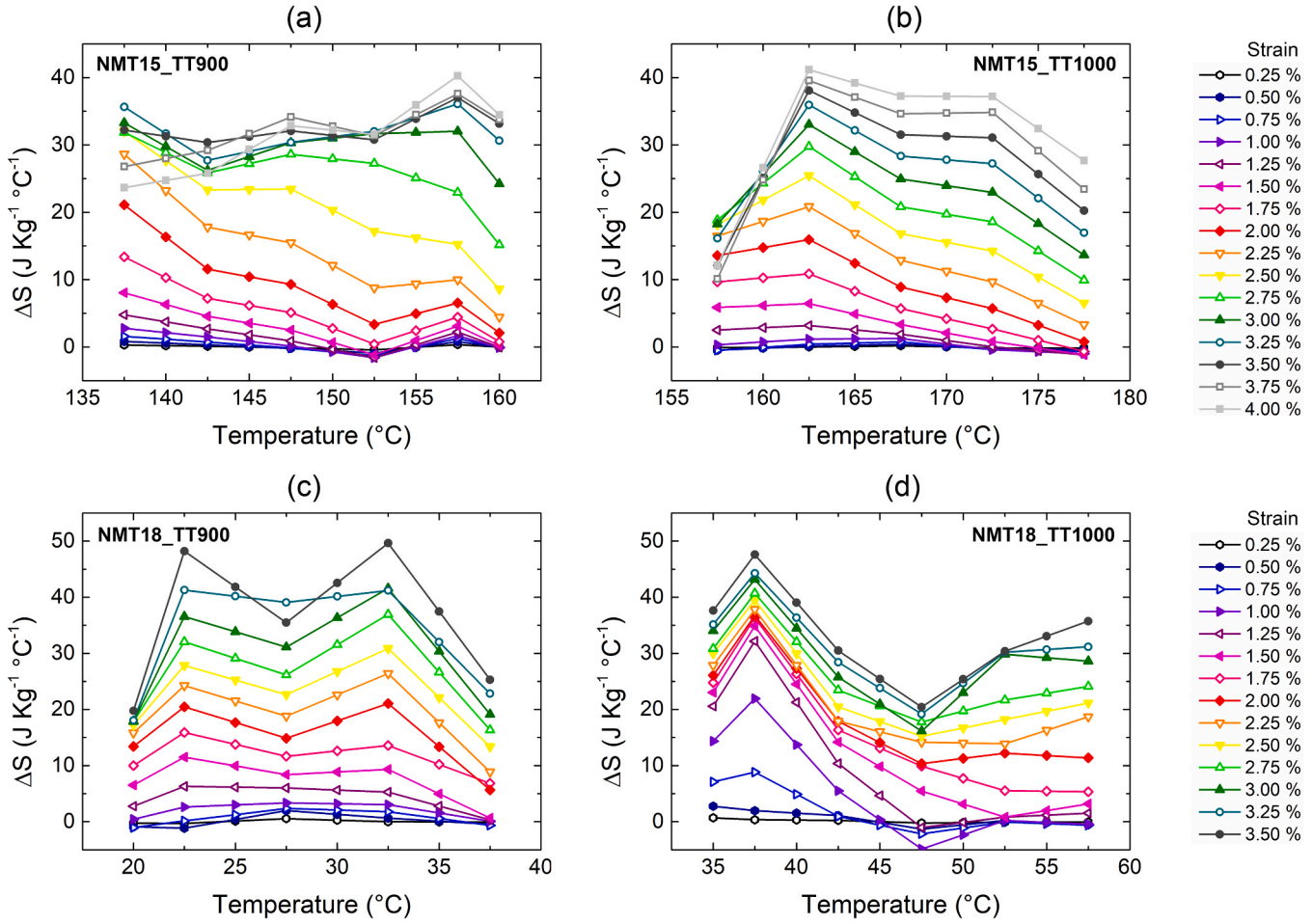

Fig. 3. Summary of the ΔS_{iso}^{SS} computed from the integration of compressive loading curves, according to Eq. 3, samples NMT15_TT900 (a), NMT15_TT1000 (b), NMT18_TT900 (c) and NMT18_TT1000 (d).

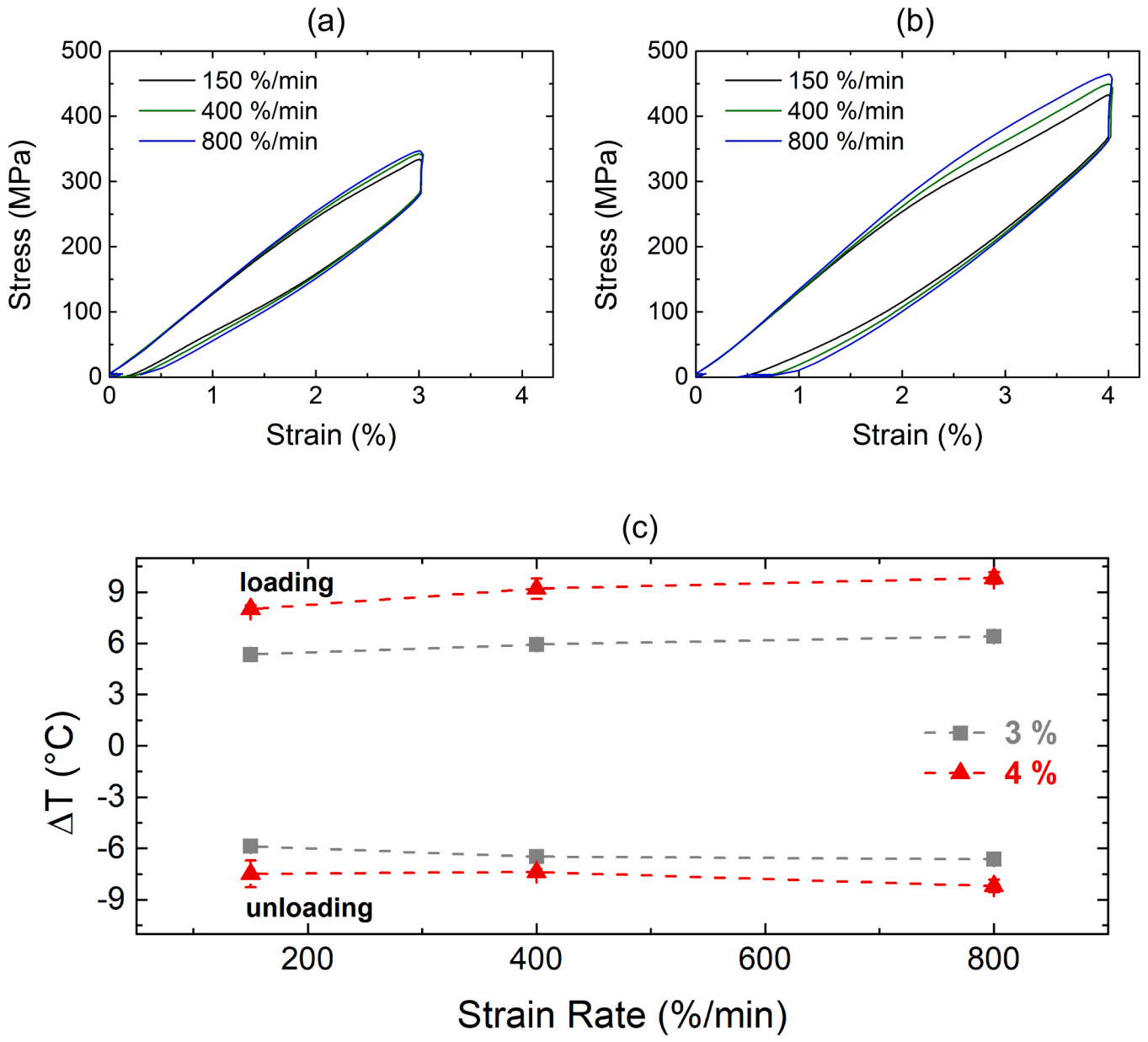

Fig. 4. Compressive adiabatic mechanical measurements at 3 % (a) and 4 % (b) of strain and summary of the mean measured adiabatic temperature changes ΔT_{ad}^{exp} in different loading conditions (c) for sample NMT18_TT900.

heat loss. In addition, the overestimation of the ΔT_{ad}^{th} obtained from calorimetry data is due to the fact that in this case the actual thermal conductivity and specific heat of the alloy are neglected and homogenous microstructural conditions are assumed [9]. In fact, the studied polycrystalline cast material is characterized by microstructural features such as grain boundaries, defects, and impurities that could affect the heat transfer properties of the alloy resulting in higher levels of dissipation [9] and in a reduction of the generated ΔT registered on the sample surface.

Fig. 7 shows that the different ΔS values have the same trend as the comparison between calorimetric and mechanical methods for ΔT calculation. The ΔS_{tr} from the thermal data is the highest possible entropy change in the thermally-induced martensitic transformation, since the whole material transforms completely by temperature change [11]. The entropy changes in isothermal conditions from mechanical stress-strain measurements (ΔS_{iso}^{CC} and ΔS_{iso}^{peak}) are lower, probably because the stress-induced martensitic transformation is not complete and homogeneous across the entire sample [9]. In addition, also in this case, the relatively limited applied strains could lead to a lower estimation of the entropy change parameter.

Considering the mechanical properties, the k_{CC} of the two alloys (Fig. 2) are higher than the typical values achieved with the NiMn-based Heusler alloys that usually range between 3 and 6 MPa °C^{-1} [30,46]. Moreover, the σ_{cr} trend exhibited by NiMnTi is more similar to that of NiTi, which can reach values up to 9 MPa °C^{-1} [9,47]. Like in NiTi, the martensitic transformation in NiMnTi alloy is sensitive to temperature and stress changes, and in the case of both NiMnTi alloys, the stress-temperature dependence is higher for the aged alloy.

Considering the effect of the two heat treatments on the mechanical and elastocaloric properties of the NiMnTi studied alloys, it was observed that the best performances were exhibited by the samples heat treated at 900 °C. In both $NiMnTi_{15}$ and $NiMnTi_{18}$ samples, martensite is induced at higher stresses (Fig. 1), and k_{CC} values are higher. This could be ascribed to the presence of NiTi-based precipitates in these samples [42,48] that could act as barriers to dislocation slip during the transition

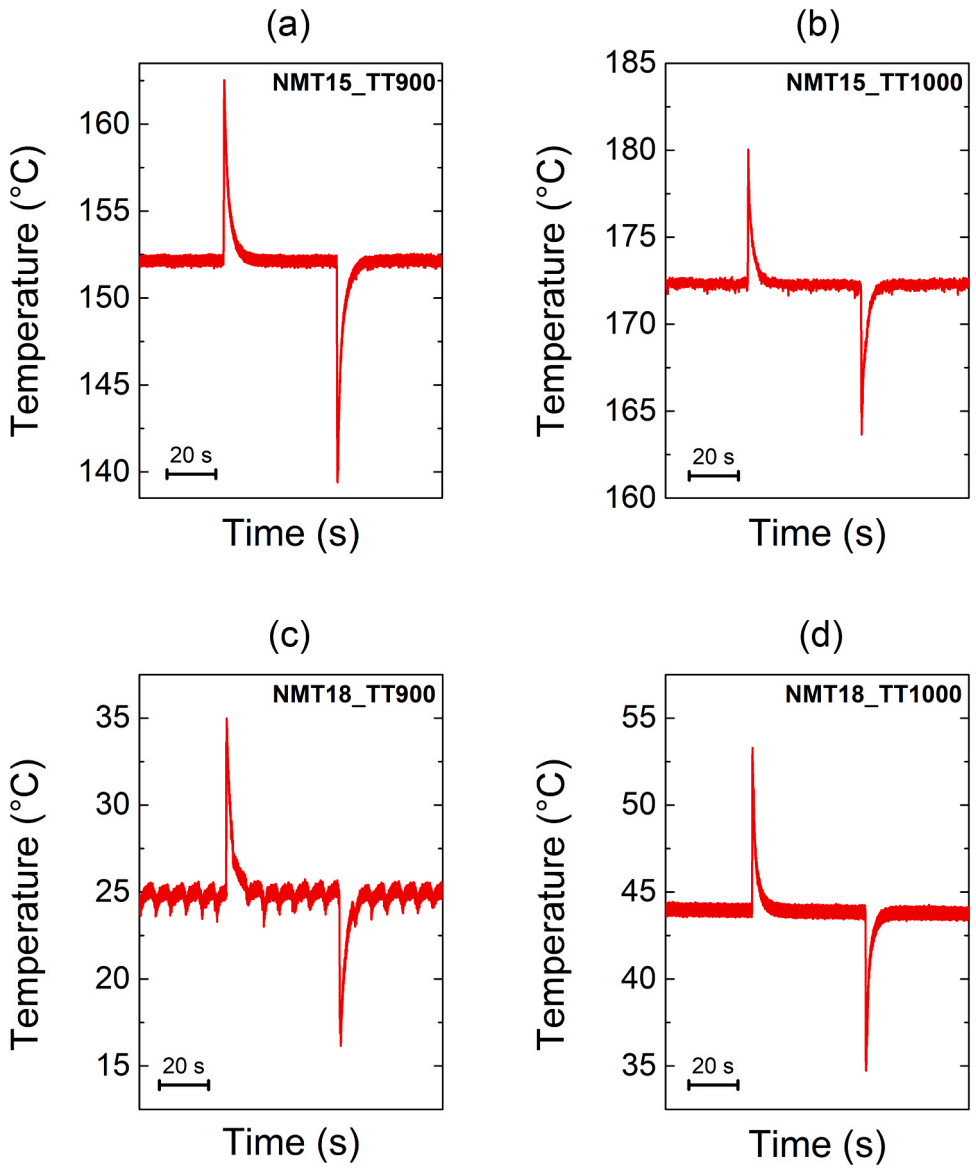

Fig. 5. Temperature profiles registered for samples NMT15_TT900 (a), NMT15_TT1000 (b), NMT18_TT900 (c) and NMT18_TT1000 (d) during compressive adiabatic mechanical measurements performed with 800 %/min strain rate up to 4 % of strain.

Table 3
Summary of the experimentally measured ΔT_{ad}^{exp} upon loading, W, and COP_{mat}.

sample	ΔT_{ad}^{exp} (loading)	W	COP_{mat} (loading)
NMT15_TT900	10.2 °C	4.7 MPa	6.8
NMT15_TT1000	7.4 °C	3.8 MPa	6.4
NMT18_TT900	9.8 °C	5.4 MPa	5.9
NMT18_TT1000	9.1 °C	5.3 MPa	5.6

from austenite to martensite [12,49]. Therefore, for these samples, higher mechanical work is necessary to induce the martensitic transformation. From all the discussed direct and indirect approaches for the determination of ΔT and ΔS, it is evidenced that the presence of precipitates in NiMnTi alloys acting as energetic barriers during the martensitic transformation is beneficial to the elastocaloric properties. This trend is confirmed by the COP_{mat} values reported in Table 3 because the best ratio between the thermal and mechanical energy for elastocaloric measurements is given by the heat treated $NiMnTi_{15}$ and $NiMnTi_{18}$ alloy with COP_{mat} values of 6.8 and 5.9, respectively. In fact, the combination between the experimental ΔT and the corresponding

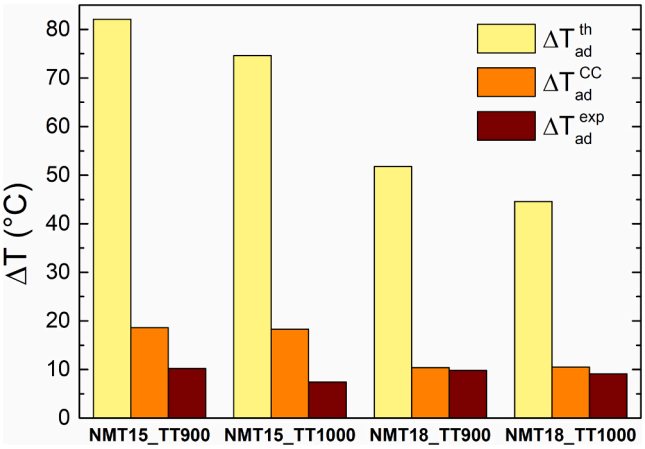

Fig. 6. Comparison of computed and experimental ΔT values.

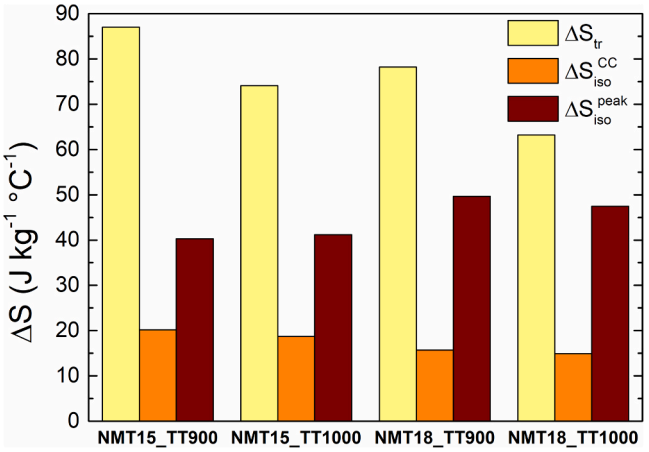

Fig. 7. Comparison of computed ΔS values from calorimetric and mechanical data.

work input is optimized in samples heat treated at 900 °C.

In summary, each sample underwent approximately 40 deformation cycles to enable the full range of characterizations presented. Preliminary assessments of the material indicate excellent mechanical stability, with no evidence of crack formation or significant plastic deformation. These findings suggest that non-textured, arc-melted NiMnTi alloy holds promising potential for elastocaloric applications. Moreover, it is possible to produce materials in relatively large bulk forms, which can then be further processed into a variety of shapes and sizes to meet specific application needs.

5. Conclusions

In this study, we investigated the mechanical and elastocaloric properties of two NiMnTi alloys with different Ti contents, fabricated by arc melting and subsequent heat treatments. We used direct and indirect methods to evaluate the adiabatic temperature change, the entropy change, and the coefficient of performance of the alloys under compressive loading. We found that the theoretical values of these parameters, derived from the calorimetric data, were significantly higher than the experimental values, due to the influence of the microstructure, the thermal properties, and the experimental conditions on the stress-induced martensitic transformation. We also found that the heat treatment at 900 °C enhanced the elastocaloric performance of both alloys. Our work provides a comprehensive analysis of the physical and functional properties of polycrystalline NiMnTi alloys produced by a melting process, considering their potential use in solid-state cooling and heat pumping technologies.

CRediT authorship contribution statement

Francesca Passaretti: Supervision, Project administration. **Riccardo Casati:** Writing – review & editing, Supervision, Conceptualization. **Francesca Villa:** Writing – original draft, Visualization, Investigation, Formal analysis, Data curation, Conceptualization. **Elena Villa:** Writing – review & editing, Supervision, Conceptualization. **Nicola Bennato:** Investigation.

Declaration of Competing Interest

The authors declare that they have no known competing financial interests or personal relationships that could have appeared to influence the work reported in this paper.

Acknowledgements

Not applicable.

Data Availability

Data will be made available on request.

References

[1] I. Takeuchi, K. Sandeman, Solid-state cooling with caloric materials, Phys. Today 68 (12) (2015) 48–54.
[2] X. Moya, N.D. Mathur, Caloric materials for cooling and heating, Science 370 (2020) 797–803.
[3] H. Mevada, B. Liu, L. Gao, Y. Hwang, I. Takeuchi, R. Radermacher, Elastocaloric cooling: a pathway towards future cooling technology, Int. J. Refrig. 162 (2024) 86–98.
[4] F. Bruederlin, L. Bumke, C. Chluba, H. Ossmer, E. Quandt, M. Kohl, Elastocaloric cooling on the miniature scale: a review on materials and device engineering, Energy Technol. 6 (2018) 1588–1604.
[5] P. Kabirifar, A. Žerovnik, Ž. Ahčin, L. Porenta, M. Brojan, J. Tušek, Elastocaloric cooling: state-of-the-art and future challenges in designing regenerative elastocaloric devices, J. Mech. Eng. 65 (11-12) (2019) 615–630.
[6] Report of the International Energy Agency (IEA) "The Future of Cooling: opportunities for energy-efficient air conditioning" (2018).
[7] L. Cirillo, A. Greco, C. Masselli, Analysis of the environmental impact of a heat pump based on the elastocaloric effect, Int. J. Refrig. 156 (2023) 161–172.
[8] C. Aprea, A. Greco, A. Maiorino, C. Masselli, The environmental impact of solid-state materials working in an active caloric refrigerator compared to a vapor compression cooler, Int. J. Heat. Technol. 36 (4) (2018) 1155–1162.
[9] Y. Wu, E. Ertekin, H. Sehitoglu, Elastocaloric cooling capacity of shape memory alloys - Role of deformation temperatures, mechanical cycling, stress hysteresis and inhomogeneity of transformation, Acta Mater. 135 (2017) 158–176.
[10] J. Chen, L. Lei, G. Fang, Elastocaloric cooling of shape memory alloys: a review, Mater. Today Commun. 28 (2021) 102706.
[11] E. Bonnot, R. Romero, L. Manosa, E. Vives, A. Planes, Elastocaloric effect associated with the martensitic transition in shape-memory alloys, Phys. Rev. Lett. 100 (2008) 125901.
[12] K. Otsuka, X. Ren, Physical metallurgy of Ti–Ni-based shape memory alloys, Prog. Mater. Sci. 50 (2005) 511–678.
[13] C. Cazorla, Novel mechanocaloric materials for solid-state cooling applications, Appl. Phys. Rev. 6 (2019) 041316.
[14] J. Tušek, K. Engelbrecht, L. Manosa, E. Vives, N. Pryds, Understanding the thermodynamic properties of the elastocaloric effect through experimentation and modelling, Shape Mem. Superelast 2 (2016) 317–329.
[15] I. Aaltio, T. Fukuda, T. Kakeshita, A perspective on elastocaloric effect in Ti–Ni-based shape memory alloys, Shape Mem. Superelast 5 (2019) 230–234.
[16] L. Manosa, A. Planes, Materials with giant mechanocaloric effects: cooling by strength, Adv. Mater. 29 (2017) 1603607.
[17] S.M. Kirsch, F. Welsch, N. Michaelis, M. Schmidt, A. Wieczorek, J. Frenzel, G. Eggeler, A. Schgtze, S. Seelecke, NiTi-based elastocaloric cooling on the macroscale: from basic concepts to realization, Energy Technol. 6 (2018) 1567–1587.
[18] S. Qian, Y. Geng, Y. Wang, J. Ling, Y. Hwang, R. Radermacher, I. Takeuchi, J. Cui, A review of elastocaloric cooling: materials, cycles and system integrations, Int. J. Refrig. 64 (2016) 1–19.
[19] S. Dall'Olio, Z. Ahčin, A. Žerovnik, P. Kabirifar, M. Brojan, J. Tušek, Development of a tube-based elastocaloric regenerator loaded in compression: a review, Shap. Mem. Superelast. (2024).
[20] G.J. Pataky, E. Ertekin, H. Sehitoglu, Elastocaloric cooling potential of NiTi, Ni2FeGa, and CoNiAl, Acta Mater. 96 (2015) 420–427.
[21] D.C. Lagoudas, Shape Memory Alloys – Modeling and Engineering Applications, Springer, New York, NY, 2008.
[22] E.M. Slyusarenko, A.V. Peristyi, E.Yu Kerimov, I.L. Guzei, M.V. Sofin, Ternary systems of nickel and manganese with transition metals, J. Alloy. Compd. 256 (1997) 115–128.
[23] E.S. Belosludtseva, N.N. Kuranova, N.I. Kourov, V.G. Pushin, A.N. Uksusnikov, Effect of titanium alloying on the structure, the phase composition, and the thermoelastic martensitic transformations in ternary Ni—Mn—Ti alloys, Tech. Phys. 60 (2015) 1330–1334.
[24] H.L. Yan, L.D. Wang, H.X. Liu, X.M. Huang, N. Jia, Z.B. Li, B. Yang, Y.D. Zhang, C. Esling, X. Zhao, L. Zuo, Giant elastocaloric effect and exceptional mechanical properties in an all-d-metal Ni–Mn–Ti alloy: experimental and ab-initio studies, Mater. Des. 184 (2019) 108180.
[25] Z.Y. Wei, E.K. Liu, J.H. Chen, Y. Li, G.D. Liu, H.Z. Luo, X.K. Xi, H.W. Zhang, W. H. Wang, G.H. Wu, Realization of multifunctional shape-memory ferromagnets in all-d-metal Heusler phases, Appl. Phys. Lett. 107 (2015) 022406.
[26] G. Li, E. Liu, G. Wu, *d-d* hybridization controlled large-volume-change martensitic phase transition in Ni-Mn-Ti-based all-*d*-metal Heusler compounds, J. Alloy. Compd. 923 (2022) 166369.
[27] G. Li, E. Liu, W. Wang, G. Wu, Theoretical investigations on elastic properties, phase stability, and magnetism in Ni2Mn-based all-*d*-metal Heusler compounds, Phys. Rev. B 107 (2023) 134440.

[28] V.G. de Paula, M.S. Reis, All-d-Metal Full Heusler Alloys: A Novel Class of Functional Materials, Chem. Mater. 33 (2021) 5483–5495.
[29] F. Villa, A. Morlotti, C. Fanciulli, F. Passaretti, F. Albertini, E. Villa, Anomalous mechanical behavior in NiMnGa alloy sintered through open die pressing method, Mater. Today Commun. 34 (2023) 105391.
[30] F. Villa, E. Bestetti, R. Frigerio, M. Caimi, C. Tomasi, F. Passaretti, E. Villa, Elastocaloric properties of polycrystalline samples of NiMnGaCu ferromagnetic shape memory alloy under compression: effect of improvement of thermoelastic martensitic transformation, Materials 150 (2022) 7123.
[31] F. Villa, A. Nespoli, C. Fanciulli, F. Passaretti, E. Villa, Physical characterization of sintered NiMnGa ferromagnetic shape memory alloy, Materials 13 (2020) 4806.
[32] D. Cong, W. Xiong, A. Planes, Y. Ren, L. Manosa, P. Cao, Z. Nie, X. Sun, Z. Yang, X. Hong, Y. Wang, Colossal elastocaloric effect in ferroelastic Ni-Mn-Ti alloys, Phys. Rev. Lett. 122 (2019) 255703.
[33] Z.Y. Wei, W. Sun, Q. Shen, Y. Shen, Y.F. Zhang, E.K. Liu, J. Liu, Elastocaloric effect of all-d-metal Heusler NiMnTi(Co) magnetic shape memory alloys by digital image correlation and infrared thermography, Appl. Phys. Lett. 114 (2019) 101903.
[34] Guoyao Zhang, Honglin Wang, Zongbin Li, Bo Yang, Haile Yan, Xiang Zhao, Liang Zuo, Colossal elastocaloric effect in a <001>A oriented Ni49Mn33Ti18 polycrystalline alloy, Scr. Mater. 234 (2023) 115584.
[35] Z. Yang, D.Y. Cong, X.M. Sun, Z.H. Nie, Y.D. Wang, Enhanced cyclability of elastocaloric effect in boron-microalloyed Ni-Mn-in magnetic shape memory alloys, Acta Mater. 127 (2017) 33–42.
[36] Z. Yang, D.Y. Cong, Y. Yuan, Y. Wu, Z.H. Nie, R.G. Li, Y.D. Wang, Ultrahigh cyclability of a large elastocaloric effect in multiferroic phase-transforming materials, Mater. Res. Lett. 7 (2019) 137–144.
[37] S. Li, D. Cong, W. Xiong, Z. Chen, X. Zhang, Z. Nie, S. Li, R. Li, Y. Wang, Y. Cao, Y. Ren, Y. Wang, A low-cost Ni−Mn−Ti−B high-temperature shape memory alloy with extraordinary functional properties, ACS Appl. Mater. Interfaces 13 (2021) 31870–31879.
[38] B. Li, Z. Liu, D. Li, Z. Feng, J. Zhu, H. Zhong, S. Li, Large reversible multicaloric effects over a broad refrigeration temperature range in Co and B co-doped Ni–Mn–Ti alloys, Mater. Sci. Eng. A 896 (2024) 146260.
[39] C. Xiong, J. Bai, Y. Li, J. Gu, X. Liang, Z. Guan, Y. Zhang, C. Esling, X. Zhao, L. Zuo, First-principles investigation on phase stability, elastic and magnetic properties of boron doping in Ni-Mn-Ti Alloy, Acta Metall. Sin. (Engl. Lett.) 35 (2022) 1175–1183.
[40] G. Zhang, H. Wang, Z. Li, B. Yang, H. Yan, L. Zuo, Giant elastocaloric effect covering a wide temperature region in a directionally solidified Ni50Mn30Ti20 alloy, Scr. Mater. 237 (2023) 115725.
[41] Z. Guan, J. Bai, Y. Zhang, J. Gu, Y. Zhang, C. Esling, X. Zhao, L. Zuo, Ultrahigh cyclic stability and giant elastocaloric effect in directionally solidified (Ni50Mn28Fe2.5Ti19.5)99.4B0.6 alloy, Scr. Mater. 229 (2023) 115353.
[42] F. Villa, E. Villa, L. Righi, P. Ruggieri, N. Bennato, S. Battiston, F. Passaretti, R. Casati, Effect of the thermal processing on the microstructural, functional and mechanical properties of cast polycrystalline NiMnTi alloys, J. Alloy. Compd. 1000 (2024) 175099.
[43] F. Villa, M. Tamandi, F. Passaretti, E. Bassani, E. Villa, Promising elastocaloric properties of sintered polycrystalline NiMnGa produced by open die pressing, J. Mater. Sci. 58 (2023) 15240–15250.
[44] F. Villa, E. Villa, E. Bassani, C. Tomasi, F. Passaretti, R. Casati, A novel sintering method for polycrystalline NiMnGa production for elastocaloric applications, J. Mater. Res. Technol. 30 (2024) 5582–5589.
[45] P. Kabirifar, J. Trojer, M. Brojan, J. Tušek, From the elastocaloric effect towards an efficient thermodynamic cycle, J. Phys. Energy 4 (2022) 044009.
[46] V.A. Chernenko, E. Villa, D. Salazar, J.M. Barandiaran, Large tensile superelasticity from intermartensitic transformations in Ni49Mn28Ga23 single crystal, Appl. Phys. Lett. 108 (2016) 071903.
[47] Y. Liu, A. Mahmud, F. Kursawe, T.H. Nam, Effect of pseudoelastic cycling on the Clausius–Clapeyron relation for stress-induced martensitic transformation in NiTi, J. Alloy. Compd. 449 (2008) 82–87.
[48] E.M. Slyusarenko, A.V. Peristyi, E.Yu Kerimov, I.L. Guzei, M.V. Sofin, Ternary systems of nickel and manganese with transition metals, J. Alloy. Compd. 256 (1997) 115–128.
[49] Muhammad Imran, Xuexi Zhang, Recent developments on the cyclic stability in elastocaloric materials, Mater. Des. 195 (2020) 109030.